Acta Crystallographica Section D
Biological Crystallography
ISSN 0907-4449

X-ray study of the conformational changes in the molecule of phosphopantetheine adenylyltransferase from *Mycobacterium tuberculosis* during the catalyzed reaction

Vladimir Timofeev,[a]* Evgenia Smirnova,[a] Larisa Chupova,[b] Roman Esipov[b] and Inna Kuranova[a]

[a]Laboratory of X-ray Analysis Methods and Synchrotron Radiation, Shubnikov Institute of Crystallography, Russian Academy of Sciences, Leninsky Prospect 59, Moscow 119333, Russian Federation, and [b]Laboratory of Biotechnology, Shemyakin–Ovchinnikov Institute of Bioorganic Chemistry, Russian Academy of Sciences, Ul. Miklukho-Maklaya 16/10, Moscow 117997, Russian Federation

Correspondence e-mail: tostars@mail.ru

Received 26 July 2012
Accepted 22 September 2012

PDB References: apo PPATMt, 4e1a; PPATMt–ATP complex, 3uc5

Structures of recombinant phosphopantetheine adenylyltransferase (PPAT) from *Mycobacterium tuberculosis* (PPATMt) in the apo form and in complex with the substrate ATP were determined at 1.62 and 1.70 Å resolution, respectively, using crystals grown in microgravity by the counter-diffusion method. The ATP molecule of the PPATMt–ATP complex was located with full occupancy in the active-site cavity. Comparison of the solved structures with previously determined structures of PPATMt complexed with the reaction product dephosphocoenzyme A (dPCoA) and the feedback inhibitor coenzyme A (CoA) was performed using superposition on C^{α} atoms. The peculiarities of the arrangement of the ligands in the active-site cavity of PPATMt are described. The conformational states of the PPAT molecule in the consequent steps of the catalyzed reaction in the apo enzyme and the enzyme–substrate and enzyme–product complexes are characterized. It is shown that the binding of ATP and dPCoA induces the rearrangement of a short part of the polypeptide chain restricting the active-site cavity in the subunits of the hexameric enzyme molecule. The changes in the quaternary structure caused by this rearrangement are accompanied by a variation of the size of the inner water-filled channel which crosses the PPAT molecule along the threefold axis of the hexamer. The molecular mechanism of the observed changes is described.

1. Introduction

Phosphopantetheine adenylyltransferases (PPATs) belong to the nucleotidyltransferase α/β phosphodiesterase superfamily (Bork *et al.*, 1995). Bacterial PPATs are involved in the five-step biosynthesis of coenzyme A (CoA) from pantothenate (vitamin B_5), cysteine and ATP (Abkido, 1967). They catalyze the penultimate step of this process: the reversible transfer of an adenylyl group from ATP to 4′-phosphopantetheine, resulting in the formation of 3′-dephosphocoenzyme A (dPCoA; Geerlof *et al.*, 1999; Brown *et al.*, 2004). In the next and final step of this pathway, phosphorylation of the 3′-ribose hydroxyl of dPCoA catalyzed by dephospho-CoA kinase produces the final product, CoA. The CoA-biosynthetic pathway, which involves several ATP molecules, is an energy-consuming process and, as in the majority of such processes, the key steps are regulated by a feedback-inhibition mechanism (Jackowski & Rock, 1984; Rock *et al.*, 2003; Miller *et al.*, 2007). The reaction catalyzed by PPAT is one of the key

steps at which the reaction rate is regulated. In the presence of excess CoA the latter binds to PPAT and thereby inhibits the process.

Study of the structure and the mechanism of action of the enzymes that participate in CoA biosynthesis is of special interest. As the principal acyl-group carrier in all living organisms, CoA takes part in numerous metabolic processes (Robishaw & Neely, 1985; Begley *et al.*, 2001). In the pathogenic bacterium *Mycobacterium tuberculosis*, reduction of the intracellular level of CoA prevents bacterial growth (Zhao *et al.*, 2003). It is known that in the highest organisms the two final steps of CoA biosynthesis are catalyzed by a single bifunctional enzyme that is not similar to PPAT (Suzuki *et al.*, 1967; Worrall & Tubbs, 1983). Taking into account the key role of the reaction catalyzed by PPAT, it may be a suitable therapeutic target for the rational design of selective inhibitors of the enzyme which may be potential antibacterial drugs. The rational approach to the synthesis of potential drugs is based on knowledge of the target protein structure.

To date, the three-dimensional structures of apo PPAT and of PPAT complexed with several functional ligands (ATP, CoA, dPCoA and PhP) have been solved for a number of bacterial enzymes. They have been most thoroughly studied for PPAT from *Escherichia coli* (PPATEc) and PPAT from *M. tuberculosis* (PPATMt), which have a high degree of homology to each other (Morris & Izard, 2004; Badger *et al.*, 2005; Takahashi *et al.*, 2004; Edwards *et al.*, 2011; Yoon *et al.*, 2011; Timofeev *et al.*, 2010, 2012). The degree of identity between these enzymes is 44% and their similarity is about 77% (Timofeev *et al.*, 2010). For PPATEc, three-dimensional structures have been determined of its complexes with ATP, 4′-phosphopantetheine, coenzyme A and dPCoA (Izard, 2002, 2003; Morris & Izard, 2004; Izard & Geerlof, 1999). Three-dimensional structures of apo PPATMt and of PPATMt complexed with CoA, dPCoA, the ATP analogue adenosine-5′-(α,β)-methylenotriphosphate (AMPcPP) and 4′-phosphopantetheine (PhP) have been determined (Morris & Izard, 2003; Timofeev *et al.*, 2010, 2012; Wubben & Mesecar, 2010, 2011).

It has been shown that the biologically active form of all known bacterial PPATs is a homohexamer with point symmetry 32 composed of two trimers (Takahashi *et al.*, 2004; Badger *et al.*, 2005; Yoon *et al.*, 2011; Edwards *et al.*, 2011). Each subunit of PPATMt contains 161 amino-acid residues. The crystallographic threefold axis coincides with the threefold axis of the hexamer. Monomers related by noncrystallographic twofold axes form dimers. There is a solvent-filled channel in the centre of the hexameric molecule. The channel passes through the whole molecule along the threefold axis and in the apo form has a diameter of about 20 Å (according to the distance between the opposite C^{α} atoms) at the surface of the molecule and a diameter of about 10 Å in the centre of the molecule at the interface between the trimers (Morris & Izard, 2004). The active sites are arranged inside the hexameric molecule and their surfaces are exposed to the central solvent-filled channel. A majority of bacterial PPATs with known three-dimensional structures bind the ligand in all six active sites (Wubben & Mesecar, 2010, 2011; Timofeev *et al.*, 2010, 2012; Takahashi *et al.*, 2004; Badger *et al.*, 2005). However, half-of-the-sites reactivity has been observed in certain PPATEc complex crystals (Izard & Geerlof, 1999; Izard, 2002, 2003). It was suggested that the reaction catalyzed by PPAT is carried out by the attack of 4′-phosphopantetheine on the α-P atom of ATP without direct involvement of the functional enzyme groups in the reaction (Izard & Geerlof, 1999).

Here, we present the crystal structure of phosphopantetheine adenylyltransferase from *M. tuberculosis* (PPATMt) in complex with one of its substrates, ATP, at 1.70 Å resolution (PDB entry 3uc5) and the crystal structure of apo PPATMt at a higher resolution of 1.62 Å (PDB entry 4e1a) compared with the previous structure at 1.99 Å resolution (PDB entry 1tfu; Morris & Izard, 2004).

The crystals used for X-ray data collection were grown on the International Space Station (ISS) in the crystallization box of the Japan Aerospace Exploration Agency (JAXA) using the counter-diffusion method (Tanaka *et al.*, 2004; Kuranova *et al.*, 2011).

With the completion of this work, three-dimensional structures of PPATMt are now known for the apo enzyme, for complexes with both of the substrates ATP and PhP (PDB entries 3uc5 and 3nbk; Wubben & Mesecar, 2010) and with the reaction product dPCoA (PDB entry 3rba; Timofeev *et al.*, 2012) as well as with the feedback inhibitor CoA (PDB entries 3lcj, 3pnb and 3rhs; Timofeev *et al.*, 2010, 2012; Wubben & Mesecar, 2011). This allowed us to compare the state of the enzyme molecule during the catalytic cycle using superposition on C^{α} atoms of the three-dimensional structures of apo PPATMt and its complexes. As a result, the conformation changes which accompany the reaction catalyzed by PPAT were revealed. It was found that the rearrangement of the short part of the polypeptide chain that restricts the active-site cavity in each subunit close to the trimer–trimer interface leads to an alteration in the quaternary structure of the hexamer. This is accompanied by a variation of the diameter of the inner solvent-filled channel in the centre of the hexamer. The molecular mechanism of the rearrangement is considered in detail.

2. Materials and methods

2.1. Construction of the producing strain ER2566/pER-PPAT

2.1.1. Amplification of the PPAT gene from genomic DNA of *M. tuberculosis*. The avirulent *M. tuberculosis* strain H37Rv was subjected to hard UV radiation and solubilized with Triton X-100 (final concentration of 1% in the mixture). The mixture (50 µl) was incubated at 368 K for 20 min, centrifuged and the supernatant was used as a template for a PCR reaction. The *kdtB* gene was amplified by PCR using the primers KDT1 (CGTAAGCTTCATATGACGGGCGCGGTAT) and KDT2 (GACAAAGCTTCTAGGTCCGTTCGGTGTTGA). The PCR mixture consisted of the template (5 µl), dNTP (8 µl; 200 µ*M*), 60 pmol of each primer, 5 U *Taq* DNA polymerase,

H_2O (26 µl) and *Taq* DNA polymerase 10× buffer (5 µl). The following thermocycle regime was used: denaturation at 366 K for 10 min, annealing at 333 K for 2 min and elongation at 345 K for 2 min (three cycles) followed by denaturation at 365 K for 1 min, annealing at 333 K for 1 min and elongation at 345 K for 1 min (50 cycles).

The PCR products were purified using a PCR purification kit (Promega) according to the manufacturer's protocol.

2.1.2. Molecular cloning. The purified PCR products were cleaved with the *Nde*I and *Hin*dIII restriction endonucleases. The reaction mixture (20 µl) consisted of 2 µl 10× buffer *R* [10 m*M* Tris–HCl (pH 8.5 at 310 K), 10 m*M* $MgCl_2$, 100 m*M* KCl, 0.1 mg ml^{-1} BSA], *Nde*I (10 U), *Hin*dIII (10 U) and 2 µg of the PCR products. The mixture was incubated at 310 K for 1.5 h. Cleavage of the pET32b(+) vector at the *Nde*I restriction site located upstream of MCS and the *Hin*dIII restriction site was performed under the same conditions. The ligation of the PCR products with cleaved ends of the pET32b(+) vector was carried out in a volume of 20 µl consisting of 2 µl of the 10× buffer for T4 DNA ligase, 2 µl 5 m*M* rATP, T4 DNA ligase (10 U) and 15 µl cleaved DNA. The obtained vector harbouring the target gene was designated pER-PPAT. Since the recognition sequence of *Nde*I includes the start codon of the thioredoxin gene, the sequences of the Trx tag and the His tag were excluded from the resulting pER-PPAT plasmid.

2.1.3. Cultivation of the producing strain. The producing strain *E. coli* ER2566/pER-PPAT was cultivated in YT medium containing ampicillin (50 µg ml^{-1}) in shake flasks at 310 K until the optical density of the culture (A_{595}) reached 1.5. Expression of the recombinant construct was induced by addition of isopropyl β-D-1-thiogalactopyranoside (IPTG) to a final concentration of 0.2 m*M* with further incubation at 310 K for 4 h. The cells were pelleted by centrifugation (5000*g* for 20 min at 277 K). PPAT was obtained in a soluble form under these conditions.

2.1.4. Isolation and purification of recombinant PPATMt. The cell pellet was resuspended in buffer solution (50 m*M* Tris–HCl pH 8.0, 5 m*M* EDTA, 1 m*M* PMSF, 5 m*M* DTT) and made to disintegrate by sonication. The cleared lysate was fractionated by anion-exchange chromatography on Q Sepharose XL resin using a 0–0.5 *M* NaCl gradient. Fractions containing PPAT were pooled and concentrated for further anion-exchange chromatography on Q Sepharose HP resin using a shallower salt gradient. Residual protein and nonprotein impurities were removed by gel filtration on Sepharose S-200. The buffer solutions used in all purification stages contained DTT (0.5 m*M*). The purified PPAT was concentrated to 17.3 mg ml^{-1} and stored at 203 K. Protein concentration in solution was determined using the Bradford assay (Bradford, 1976). As shown by Timofeev *et al.* (2010), protein purified as described above was electrophoretically homogeneous.

The activity of PPAT was assayed by detecting the release of ATP in a reverse reaction catalyzed by PPAT (Lamprecht & Trautschold, 1974): dPCoA + PP_i $\longleftrightarrow$ PhP + ATP. The ATP concentration was determined indirectly by measuring NADPH formation in a coupled reaction:

$$\text{ATP} + \text{glucose} \xrightarrow{\text{hexokinase}} \text{glucose-6-phosphate} + \text{ADP}$$

$$\text{glucose-6-phosphate} + \text{NADP} \xrightarrow{\text{glucose-6-phosphate dehydrogenase}} \text{NADPH} + \text{6-phosphogluconolactone}.$$

The NADPH extinction coefficient at 340 nm (298 K) is 6220 M^{-1} cm^{-1}. One unit of activity corresponds to the formation of 1 µmol of NADPH per minute per milligram of protein per millitre. The assay mixture consisted of Tris–HCl pH 8.0 (50 m*M*), DTT (1 m*M*), $MgCl_2$ (2.0 m*M*), PP_i (2 m*M*), NADP (1.0 m*M*), dCoA (0.1 m*M*), hexokinase (3 U ml^{-1}) and glucose-6-phosphate dehydrogenase (3 U ml^{-1}). The specific activity of the recombinant PPAT was 39 U mg^{-1}.

2.2. Crystallization of apo PPATMt and PPATMt–ATP

In addition to crystals of PPATMt–dPCoA (Kuranova *et al.*, 2011), crystals of apo PPATMt and of the PPATMt–ATP complex were grown in the microgravity environment on the ISS at 293 K using the crystallization facilities of the Japan Aerospace Exploration Agency (JAXA) and the support service provided by JAXA (Sato *et al.*, 2006) during the JAXA-PCG experiment. Crystal growth was carried out by the counter-diffusion technique in a capillary over a gel layer as developed by García-Ruiz and Moreno (García-Ruiz & Moreno, 1994; García-Ruiz, 2003). The JAXA Crystallization Box (JCB), a modification of the original capillary counter-diffusion method, was used as a crystallization device (Tanaka *et al.*, 2004; Takahashi *et al.*, 2010).

A thick-walled glass capillary of 0.5 mm inner diameter and 60 mm in length was loaded with a solution of the protein in 10 m*M* HEPES buffer pH 8 to a height of 40 mm (about 8 µl protein solution). The top end of the capillary was sealed with plasticine. The other end of the capillary was inserted into a silicone tube filled with 1% agarose gel and preliminarily equilibrated in buffer solution. The end of the silicone tube was cut to a length of 5 mm. The capillary with the attached tube was firmly placed into a cylinder of 180 µl volume filled with one half of the precipitant solution. The bottom of the cylinder was closed with the cap provided with microholes in order to remove air and excess precipitant solution. All connections in the device were then thoroughly sealed with Araldite glue. The JAXA crystallization boxes (JCBs) containing the six items described above were packed hermetically into plastic boxes and were delivered to the ISS in a temperature-controlled bag by a Russian spacecraft. Crystals of the apo enzyme were grown from a solution of protein (concentration 12 mg ml^{-1}) in 10 m*M* HEPES buffer pH 8.0 containing 0.15 *M* NaCl and 1 m*M* dithiothreitol (DTT) (Kuranova *et al.*, 2011). A 1:1 mixture of the above solution with 40 m*M* cacodylate buffer pH 5.5 containing 10 m*M* $MgCl_2$, 0.15 m*M* NaCl, 20 m*M* cobalt hexamine and 15% MPD was used as precipitant solution. 14 m*M* ATP was added to the protein and precipitant solutions in order to grow crystals of the PPATMt–ATP complex. Crystals of PPAT–ATP grown in the capillary are shown in Supplementary Fig. S1.

Table 1
Data-collection and refinement statistics for apo PPATMt (PDB entry 4e1a) and PPATMt–ATP (PDB entry 3uc5) crystals.

Values in parentheses are for the last resolution shell.

PDB code	4e1a	3uc5
Data collection		
Space group	*H*32	*H*32
Unit-cell parameters (Å)	a = 98.7, c = 113.6	a = 99.9, c = 114.4
No. of molecules per asymmetric unit	1	1
Resolution (Å)	30.00–1.62 (1.66–1.62)	50.00–1.70 (1.74–1.70)
No. of unique reflections	27236	24361
Multiplicity	13.8 (7.1)	11.3 (3.9)
Completeness of data (%)	99.8 (100.0)	99.5 (99.2)
$R_{\rm merge}$ (%)	5.9 (40.2)	6.3 (42.5)
$\langle I/\sigma(I)\rangle$	51.03 (3.59)	69.51 (2.82)
Refinement		
Resolution (Å)	1.62	1.70
No. of reflections in refinement	25758	23043
No. of reflections in the test set (5%)	1381	1213
No. of refined non-H atoms in the protein molecule	1223	1219
No. of refined water molecules	147	92
No. of refined ATP atoms	—	31
No. of refined glycerol atoms	6	—
$R_{\rm cryst}/R_{\rm free}$ (%)	16.8/20.3	16.9/20.7
R.m.s.d. bond lengths (Å)	0.008	0.009
R.m.s.d. angles (°)	1.097	1.329
Average temperature factors (Å^2)		
Main chain	30.81	46.52
Side chains and protein-bound waters	37.97	51.70
All atoms	34.65	49.26
Ramachandran statistics (%)		
Most favoured regions	96.6	95.3
Additional allowed regions	3.4	4.7

2.3. X-ray data collection

X-ray data sets were collected from space-grown crystals of apo PPATMt and the PPATMt–ATP complex at 100 K on beamline BL41XU at the SPring-8 synchrotron-radiation facility in Japan equipped with an MX225HE CCD detector. Prior to flash-cooling, the crystals were soaked for a short time in cryoprotectant solution. The cryosolution consisted of the precipitant solution with 20% glycerol; the cryosolution for PPATMt–ATP additionally contained 14 m*M* ATP.

X-ray data were collected from a single crystal of apo PPATMt and of the PPATMt–ATP complex using the rotation method at a wavelength of 0.8 Å; the rotation angle was 360° for apo PPATMt and 180° for PPATMt–ATP, the oscillation angle was 0.5° and the crystal-to-detector distance was 200 mm. The experimental intensities were processed using the *HKL*-2000 program package (Otwinowski & Minor, 1997) to 1.62 Å resolution for apo PPATMt and to 1.70 Å resolution for PPATMt–ATP. The diffraction images were integrated and scaled. All crystals belonged to space group *H*32. The data-processing statistics are given in Table 1.

2.4. Structure solution and refinement

Both crystal structures were solved by the molecular-replacement method using *Phaser* (McCoy *et al.*, 2005) with the atomic coordinates of the apoenzyme at 1.99 Å resolution (PDB entry 1tfu; Morris & Izard, 2004) as a search model. Structure refinement was carried out using *REFMAC* (Murshudov *et al.*, 2011) and *PHENIX* (Adams *et al.*, 2002). Manual rebuilding of the models was performed using the *Coot* interactive graphics program (Emsley & Cowtan, 2004) and electron-density maps were calculated with $2|F_{\rm o}| - |F_{\rm c}|$ and $|F_{\rm o}| - |F_{\rm c}|$ coefficients; water molecules were located in difference electron-density maps. The position of ATP in the active site of the PPAT–ATP complex was determined. The ATP molecule was refined with full occupancy to an average B factor of 50.51 Å^2, whereas the mean B factor of the overall structure refined to 49.26 Å^2. The structure-refinement statistics are summarized in Table 1. The atomic coordinates of apo PPATMt and PPATMt–ATP have been deposited in the Protein Data Bank (PDB entries 4e1a and 3uc5, respectively).

3. Results and discussion

3.1. Quality of the crystals and quality of the model

Crystals of PPATMt and the PPATMt–ATP complex grown in microgravity by the counter-diffusion technique reached dimensions of 0.3 mm (Supplementary Fig. S1). The crystals grown in space diffracted to 0.2–0.4 Å higher resolution than the control ground crystals (Kuranova *et al.*, 2011) and were used for X-ray data collection at the SPring-8 synchrotron-radiation facility. All crystals of PPATMt belonged to space group *H*32 and contained one subunit in the asymmetric unit. X-ray data collected from space-grown crystals allowed the determination of the structure of apo PPATMt at 1.62 Å resolution and of the structure of PPATMt–ATP at 1.70 Å resolution. The electron-density map calculated with coefficients $2|F_{\rm o}| - |F_{\rm c}|$ showed clear density for the backbone, the majority of the amino-acid side chains and for a number of water molecules, but density was absent for three C-terminal amino-acid residues and for some residues in one of the irregular loops (residues 37–43). All residues of this loop have high B-factor values. Residues 40–42 were not visible in the electron-density map when it was contoured at the 1.0σ level.

3.2. Some peculiarities of the apo PPATMt structure

The apo PPATMt homohexamer is shown in Supplementary Fig. S2 as surface representations along and across the crystallographic threefold axis, which coincides with the threefold axis of the oligomer. The monomers are related by the threefold axis to form trimers related by the twofold axes to form dimers. A solvent-filled channel in the centre of the molecule provides delivery of the substrates to the active sites located on the surface of the molecule inside the channel. The

diameter of the channel becomes narrower in the direction from the surface to the centre of the molecule.

The main difference between the structures of apo PPATMt at 1.99 Å resolution (PDB entry 1tfu) and at 1.62 Å resolution (PDB entry 4e1a) is an increase in the number of ordered water molecules that are located within the active-site cavity. The secondary structure of the PPATMt subunit with water molecules in the active-site cavity is shown in Fig. 1. A five-stranded parallel β-sheet and six α-helices are folded as in the nucleotide-binding domain (Rossmann *et al.*, 1975). The active-site cavity is limited by β-strands β1, β4 and β5, α-helices α1 and α4, the N-terminal parts of helices α3 and α5 and several irregular loops. Well ordered water molecules bound by hydrogen bonds to each other and to the enzyme amino-acid residues form two clusters within the active-site cavity. It is evident that these clusters would be partly changed and rearranged upon ligand binding. This implies that there is a substantial entropic component during binding. A little heat associated with the binding process, as measured directly in isothermal titration calorimetry experiments (Wubben & Mesecar, 2010), corresponds well to this suggestion.

Of the several irregular loops which restrict the active-site area in the PPAT subunit, at least two play significant roles in the action of PPAT (Izard & Geerlof, 1999; Timofeev *et al.*, 2010; Wubben & Mesecar, 2010). It has been shown that the movement of these loops upon ligand binding affects the rate-determining step of the kinetic mechanism and contributes to the regulation of the rate of the whole biosynthetic pathway (Wubben & Mesecar, 2010). The arrangement of these two functionally important loops in PPATMt dimers and trimers is shown in Supplementary Fig. S3. A long flexible loop I (residues 37–46) situated between strand β2 and helix α2 restricts (together with helix α5) the entrance into the solvent-filled channel. The entrance into the channel is a functionally important part of the molecule. The amino-acid residues arranged around the perimeter of the solvent-filled channel are able to influence the rate of ligand delivery and binding to the active site (Morris & Izard, 2004). Loop I contains the functionally important lysine residue (Lys42 in PPATEc and Lys41 in PPATMt; Izard & Geerlof, 1999; Izard, 2002). This lysine has been suggested to take part in stabilization of the pentacovalent transition state which forms after the attack on the α-phosphate of ATP (Morris & Izard, 2004). However, loop I is very weakly located in the electron-density map in the majority of PPATs with known three-dimensional structures, including PPATMt. This loop is only definitely fixed in the PPATEc–ATP and PPATEc–PhP complexes (Izard, 2002). In apo PPATMt electron density for residues 40–42 is completely absent, whereas residues 43–46 are characterized by high *B*-factor values.

The short loop II (residues 89–94) is situated between strand β4 and helix α4 at the bottom of the active site. In the hexameric PPATMt molecule these loops form the perimeter of the solvent-filled channel in the centre of the molecule near the trimer–trimer interface (Supplementary Fig. S3). Loop II contains the functionally important residue Arg90 and changes its conformation upon the binding of ligands (Izard, 2003; Wubben & Mesecar, 2010; Timofeev *et al.*, 2012). In apo PPATMt the guanidino group and main-chain O atom of Arg90 form hydrogen bonds to Thr91 and Thr93, whereas Glu96 and Asp94 are exposed to the channel, providing a

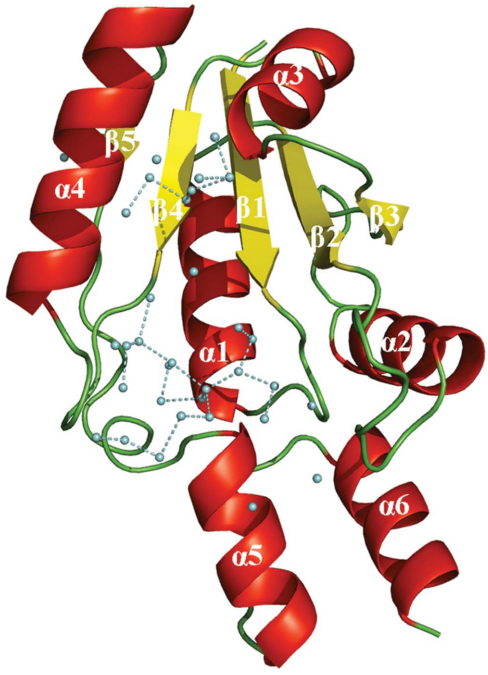

Figure 1
The subunit of PPATMt with two clusters of water molecules in the active-site cavity. Helices are coloured red, β-strands yellow and irregular loops green. Water molecules are shown as cyan spheres and hydrogen bonds are shown as dashed lines.

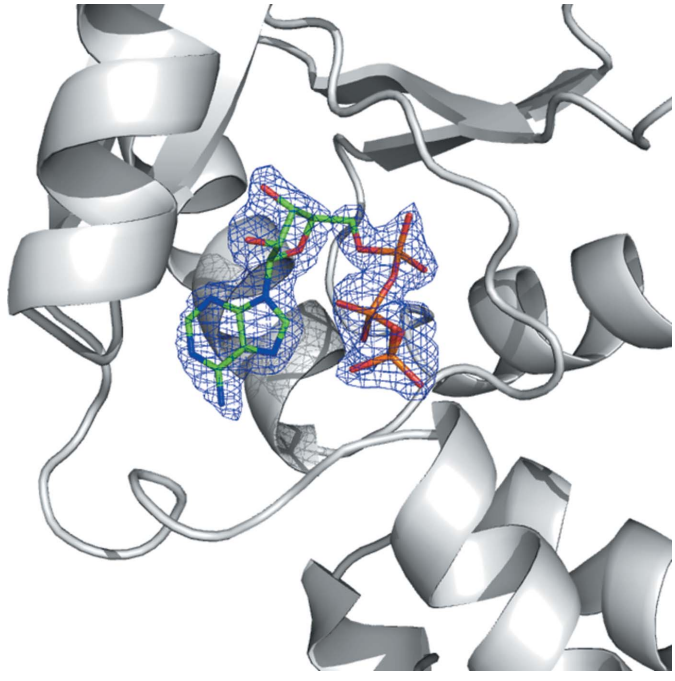

Figure 2
The arrangement of the ATP molecule in the active site of the PPATMt subunit. The electron-density map for ATP was calculated without ligand with coefficients $2|F_o| - |F_c|$ and is contoured at 1.0σ.

strong negative charge near the trimer–trimer interface. Unlike PPATEc, in which the amino-acid residues in this region have high *B*-factor values, the residues of loop II in PPATMt fit very well into the electron density and have *B* factors that are comparable with the average values for the whole molecule. The role of loop II in the function of the enzyme will be considered below.

3.3. The three-dimensional structure of PPATMt–ATP

The ATP molecule fitted into the electron density of the PPATMt subunit is shown in Fig. 2. The electron-density map for ATP was calculated without ligand with coefficients $2|F_o| - |F_c|$ and was contoured at 1.0σ. The ATP molecule bound in the active site is partially separated from the surface of the hexamer by the weakly located flexible loop I and helix $\alpha5$. The adenylyl group of ATP is arranged close to the bottom of the active site near the trimer–trimer interface. The nearest environment of ATP is shown in Fig. 3. The adenine ring hydrogen-bonds directly to Tyr118, Tyr122 and Val125 and *via* water molecules to Thr14, His17, Ala119, Ser127, Ser128 and Asp19. Two ribose hydroxyls are bound to the carbonyl O atom of Gly88 ($\beta4$ strand); for one of these the 3′-hydroxyl additionally binds to the side chain of Glu98. The phosphate groups of ATP are fixed rather strongly owing to a network of hydrogen bonds (direct or water-mediated). The α-phos--phosphate O atoms are bound directly and through water molecules to His17 $N^{\varepsilon2}$, the γ-OH of Ser9, the main-chain N atom of Phe10 and to three ordered water molecules. The β- and γ-phosphates are exposed to the solvent channel. The O atoms of the β-phosphate are bound to His17 $N^{\varepsilon2}$ and two N atoms of the guanidine group of Arg90. The O atoms of γ-phosphate interact with the guanidine group of Arg90 and the main-chain N atoms of Ser128 and Arg90. Thus, several amino-acid residues that are invariant in the majority of bacterial PPATs (Val125, Tyr122, His17, Arg90, Glu8, Ser9, Phe10, Asp19 and Ser128) participate in the binding of ATP. A very similar position in PPATMt is occupied by the ATP-molecule

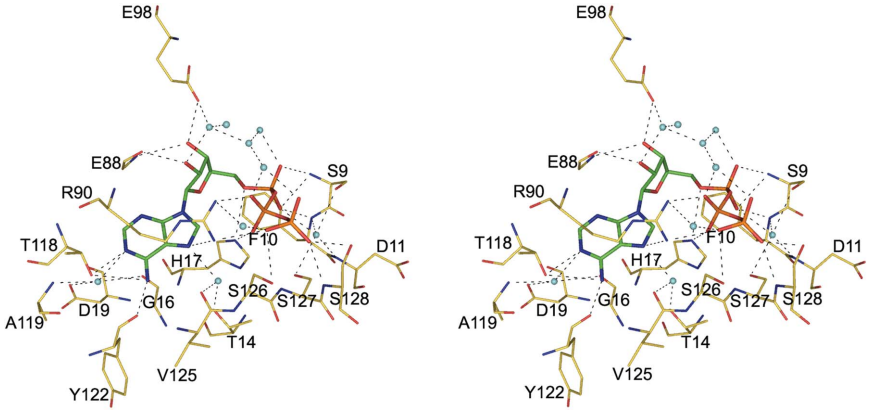

Figure 3
Stereoview of the environment of ATP in the PPATMt subunit. The ATP molecule and amino-acid residues are coloured according to atom type. Hydrogen bonds are shown as dashed lines. Water molecules are shown as cyan spheres.

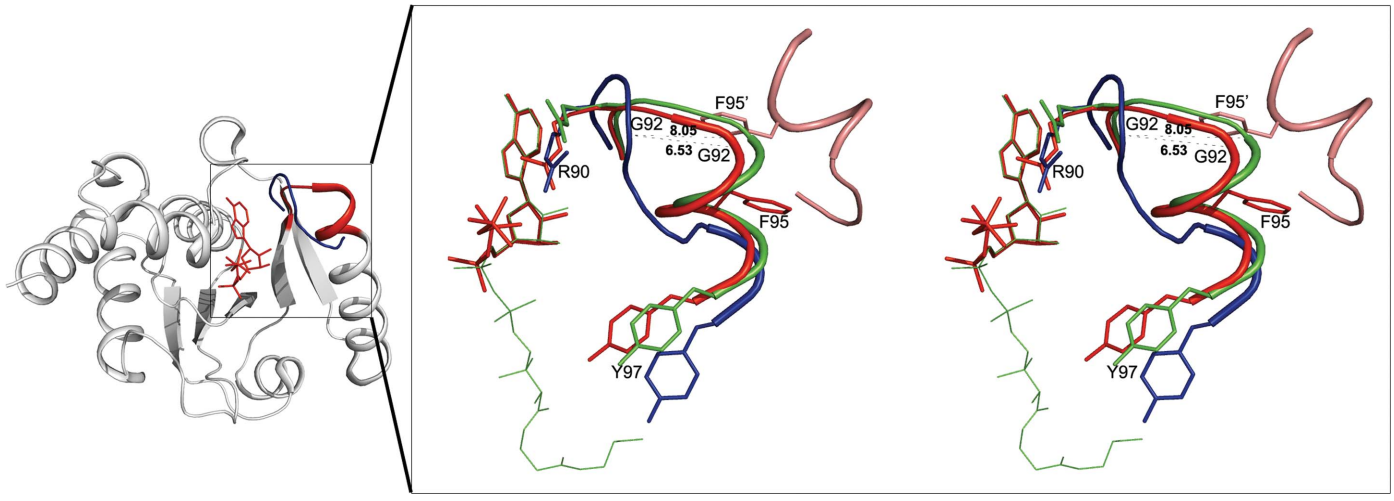

Figure 4
The conformational changes in the region 89–97 of the PPATMt subunit upon binding of ATP and dPCoA. In the inset on the left the region 89–97 of apo PPATMt is shown in blue; the same region in PPATMt–ATP and the ATP molecule are shown in red. In the stereoview on the right the polypeptide chain 89–97 in apo PPAT is coloured blue, that in PPATMt–ATP is coloured red and that in PPATMt–dPCoA is coloured green. Polypeptide chains are shown in cartoon representation; the ligand molecules and amino-acid side chains are shown as sticks. The ATP molecule is coloured red and the dPCoA molecule is coloured green. The subunit across the dyad axis is shown as a salmon cartoon. The distances between the C^{α} atoms of Gly92 in different forms of PPATMt are shown in Å.

analogue AMPcPP (PDB entry 3nba; Wubben & Mesecar, 2011). A slight difference in the positions of several atoms of the phosphates is possibly a consequence of the differing resolutions (1.62 Å for PPATMt–ATP and 2.68 Å for PPATMt–AMPcPP).

3.4. The conformational changes of the PPATMt molecule during the catalyzed reaction: comparison of apo PPATMt with PPATMt–ATP, PPATMt–dPCoA and PPATMt–CoA

The three-dimensional structures of PPATMt presently known for the apo-enzyme and for the enzyme complexed with the substrates ATP and PhP, the product dPCoA and the feedback inhibitor CoA provide an opportunity to determine the state of the enzyme molecule at several steps of the catalyzed reaction using superposition on the C^{α} atoms.

The conformational changes in the subunit of apo PPATMt upon ATP and dPCoA binding are shown in Fig. 4. These changes are concentrated in the region of residues 89–96 of each subunit. As mentioned above, in the hexameric enzyme residues 89–96 are situated at the perimeter of the solvent channel near the interface of the dimer and trimer (Fig. 5, Supplementary Fig. S3). Because of this, variation in these regions promotes changes in the contacts between the subunits of the hexamer and, as a consequence, in the quaternary structure of the enzyme. The surroundings of the solvent channel in apo-form PPATMt and in its complexes are shown in Fig. 5.

When an ATP molecule binds to the enzyme, residue Arg90, which is hydrogen-bonded to the main-chain O atoms of Thr91 and Thr93 in the apoenzyme, moves to form hydrogen bonds to the O atoms of the β- and γ-phosphates of ATP. This movement increases the space for the accommodation of the adenylyl group of ATP. The shift of the main-chain O atom of Arg90 reaches 1.55 Å; the shift of the C^{ζ} atom of the guanidine group is 1.69 Å. When the hydrogen bonds between Arg90 and residues Thr91 and Thr93 are broken, the whole region 89–96 undergoes significant rearrangement (Fig. 4). The polypeptide chain of region 89–94 moves and twists in such a way that residues 89–92 form an almost complete additional turn at the N-terminus of the α4 helix.

The side chain of Asp94 hydrogen-bonds to the guanidine group and main-chain N atom of Arg90 and the O^{γ} and main-chain N atoms of Thr91. As a result, the side chain of Thr93 is now directed into the solvent-filled channel and forms

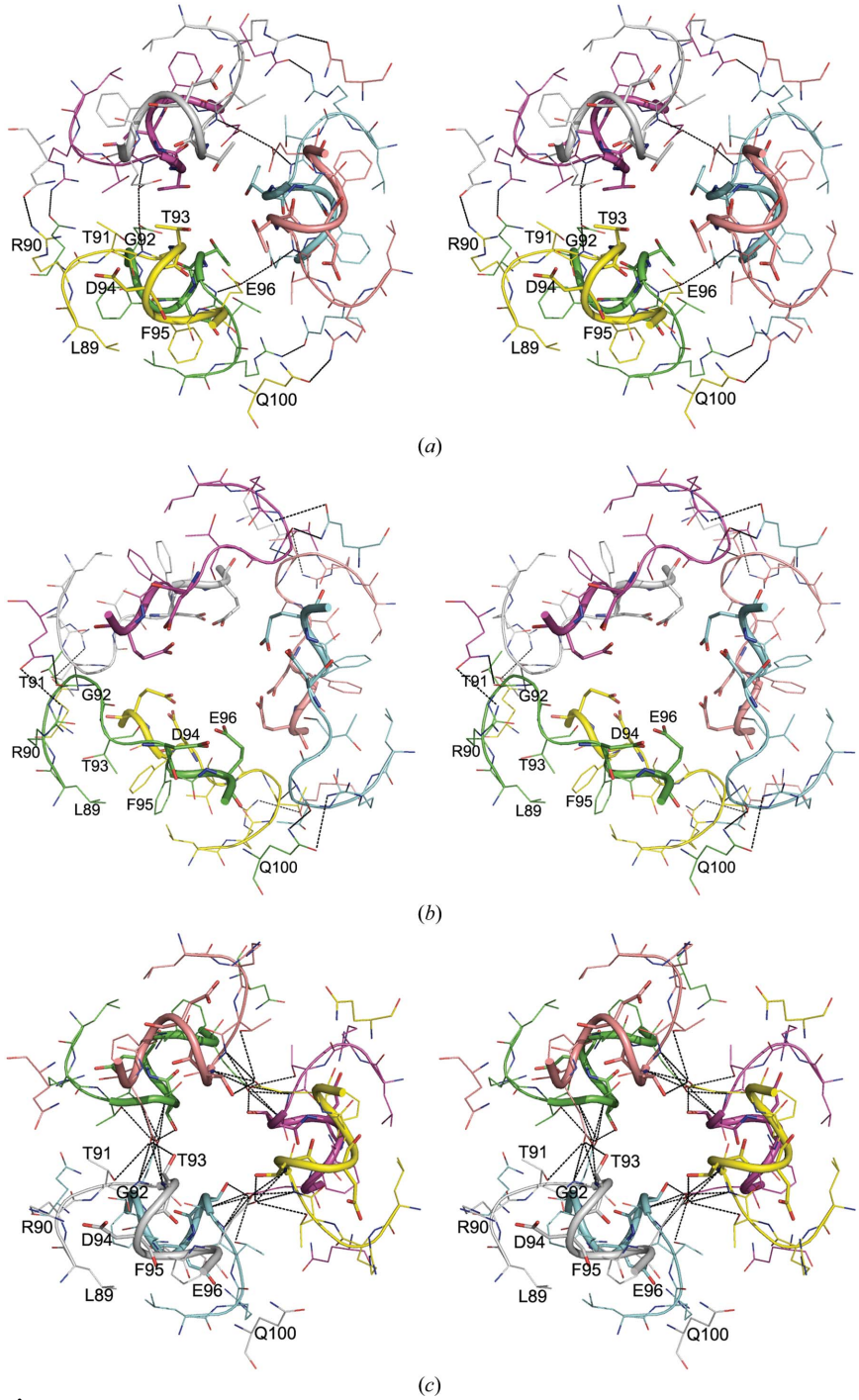

Figure 5
The changes in the quaternary structure of PPATMt upon ligand binding. The regions 89–96 that surround the solvent-filled channel near the trimer–trimer interface are presented in the different forms of the PPATMt hexamer: (*a*) in the apoenzyme, (*b*) in PPATMt–ATP and (*c*) in PPATMt–dPCoA. The stereoview is down the triad axis of the hexamer. The subunits are shown in different colours. The polypeptide chain is shown in cartoon representation, the helical part is shown in bold cartoon representation and amino-acid residues are shown as sticks. The amino-acid side chains directed into the solvent channel or arranged along its perimeter are shown as bold sticks. Hydrogen bonds are shown as dashed lines.

hydrogen bonds to the carboxylic group of Glu96″ of the adjacent subunit of the second trimer (Thr93 O^{γ}—Glu96″ $O^{\varepsilon1}$; Thr93 N—Glu96″ $O^{\varepsilon1}$ and $O^{\varepsilon2}$). The largest shift of 6.53 Å is observed for the C^{α} atom of Gly92. The side chains of Glu96 in the apoenzyme are exposed to the channel and provide a strong negative charge in the channel near the trimer–trimer interface (Fig. 5*a*). In PPATMt–ATP the carboxylic O atoms of Glu96 form hydrogen bonds to the main-chain N atoms of Gly92, Thr91 and Thr93 of the neighbouring subunit and the local negative charge inside the channel near the trimer interface is significantly reduced (Fig. 5*b*).

A very similar rearrangement of region 89–96 was found when apo PPATMt binds the ATP analogue α,β-methyleneadenosine triphosphate (Wubben & Mesecar, 2010). The conformation of the homologous region in PPATEc–ATP (Izard, 2002) is also rather similar to that described above.

The region 89–96 of PPATMt–dPCoA is shown in Fig. 5(*c*). The structure of PPATMt with the reaction product 3′-dephosphocoenzyme has been determined at 1.59 Å resolution (PDB entry 3rba; Timofeev *et al.*, 2012). It was shown that the molecule of dPCoA is accommodated in the elongated cavity which extends from the surface towards the centre of the hexamer. Unlike PPATEc, in which dPCoA was found only in one of two trimers (Izard & Geerlof, 1999; Izard, 2003), dPCoA is located in each subunit of the PPATMt hexamer. The position of the phosphopantetheine arm in PPATMt–dPCoA is very similar to its position in PPATEc–dPCoA and to the positions of the 4′-phosphopantetheine molecule complexed with PPAT from *Thermus thermophilus* and with PPATMt (Izard & Geerlof, 1999; Takahashi *et al.*, 2004; Wubben & Mesecar, 2010).

The superposition of the structures of PPATMt–ATP and PPATMt–dPCoA on C^{α} atoms reveals that the conformations of regions 89–96 of the structures are similar but not identical (Figs. 4 and 5). There is a difference in the positions of some important residues, especially Arg90. As a consequence of the lack of hydrogen bonds to the O atoms of the β- and γ-phosphate of ATPs, Arg90 is shifted closer to the water-filled channel, whereas its previous position is occupied by water molecules. The shift of the guanidine group of Arg90 in PPATMt–dPCoA relative to its position in PPATMt–ATP exceeds 3 Å. The guanidine group of Arg90 in PPATMt–dPCoA forms a direct hydrogen bond to the main-chain O atom of Ser123 and forms water-mediated hydrogen bonds to the adenine ring and Asp94 $O^{\delta1}$. Another hydrogen bond is formed between the main-chain N atom of Arg90 and Asp94 $O^{\delta1}$. The side chain of Thr93, which is involved in the hydrogen-bond system in PPAT–ATP, is exposed directly to the solvent channel in PPATMt–dPCoA (Fig. 5).

Besides the shifts of some amino-acid residues inside the subunit and on the perimeter of the solvent channel, some changes are observed in the interface between the subunits of

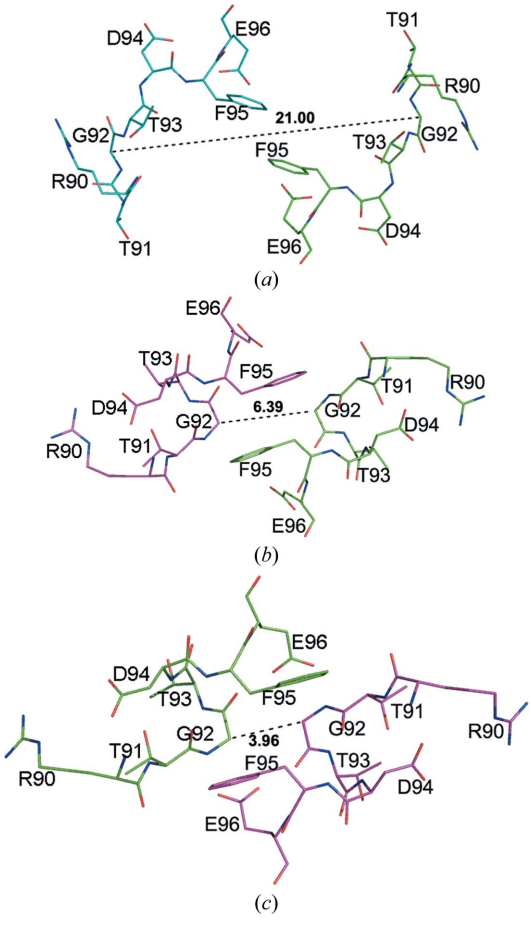

Figure 6
Conformational changes in the dimer interface of PPATMt. Region 90–96 is shown for (*a*) the apoenzyme, (*b*) PPAT–ATP and (*c*) PPAT–dPCoA. The distances between the C^{α} atoms of the Gly92 residues of the dimers (dashed lines) are shown in Å.

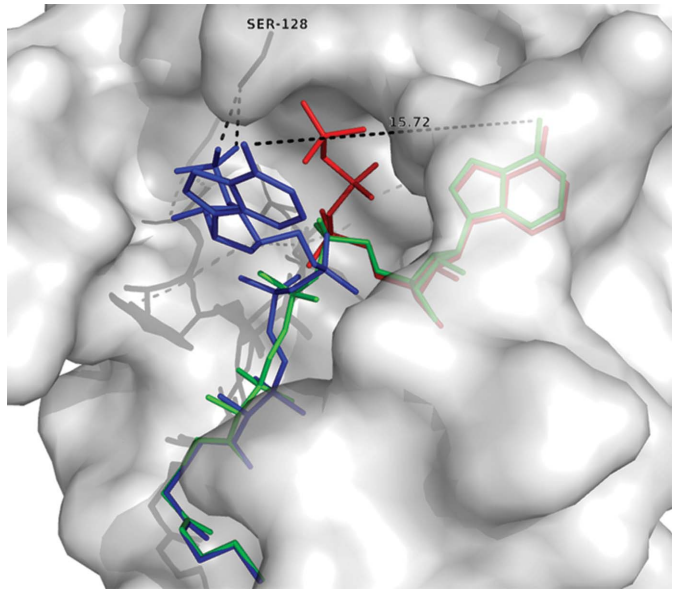

Figure 7
Comparison of the positions of substrate (ATP, red sticks), product (dPCoA, green sticks) and feedback inhibitor (CoA, blue sticks) in the PPATMt subunit. The structures of PPATMt–ATP (PDB entry 3uc5), PPATMt–dPCoA (PDB entry 3rba) and PPATMt–CoA (PDB entry 3rhs) are superimposed on C^{α} atoms. The distance between the adenylate NH_2 groups of ATP and CoA (labelled in Å) as well as the hydrogen bonds between the 3′-phosphate and Ser128 are shown as dashed lines. The enzyme molecule is shown as a surface representation.

the dimers in the different forms of PPATMt (Fig. 6). After the formation of an additional turn at the α4 N-terminus, new contacts appear between the α4 helices of neighbouring subunits and the distance between the Gly92 residues in the subunits across the twofold axis changes from 21.00 Å in the apo form to 6.39 and 3.96 Å in PPATMt–ATP and PPATMt–dPCoA, respectively.

From a comparison of the structures of PPATMt complexed with functional ligands, structural changes in PPATMt take place upon the binding of ATP and dPCoA but do not occur upon binding the feedback inhibitor CoA and PhP. Moreover, whereas the positions of the adenylate groups of dPCoA and ATP nearly coincide in PPATMt, they differ drastically from the position of the adenylate in PPATMt–CoA (Fig. 7). The adenine ring of CoA is almost completely exposed to the solvent-filled channel, does not interact with any groups of the enzyme and is very weakly visible in the electron-density map (Timofeev *et al.*, 2010, 2012). The positions of the phosphopantetheine arm of CoA and dPCoA nearly coincide; the distance between the amino groups of the adenine rings in the corresponding complexes with PPATMt is 15.72 Å.

CoA and dPCoA molecules differ only by the presence of a phosphate group at the 3′-position of the ribose ring in CoA. It is probably just this difference that leads to the dramatic changes in the location of the adenylyl group in the corresponding complexes. In PPATMt the O atoms of the 3′-phosphate group form hydrogen bonds to the cluster of invariant serine residues 126–128. These bonds fix the ribose ring in a new position and the adenylyl group of CoA cannot penetrate deeply into the active site and occupy the space near Arg90. In the *E. coli* enzyme, in which density for the adenylyl group of CoA is found in only one of the trimers, the 3′-phosphate group binds to Arg91 and the adenylate ring forms a stacking interaction with the side chain of Tyr98 (Izard, 2003; Supplementary Fig. S4). Owing to this, the adenylate is located slightly deeper, although as in PPATMt it is directed into the solvent channel. This finding correlates

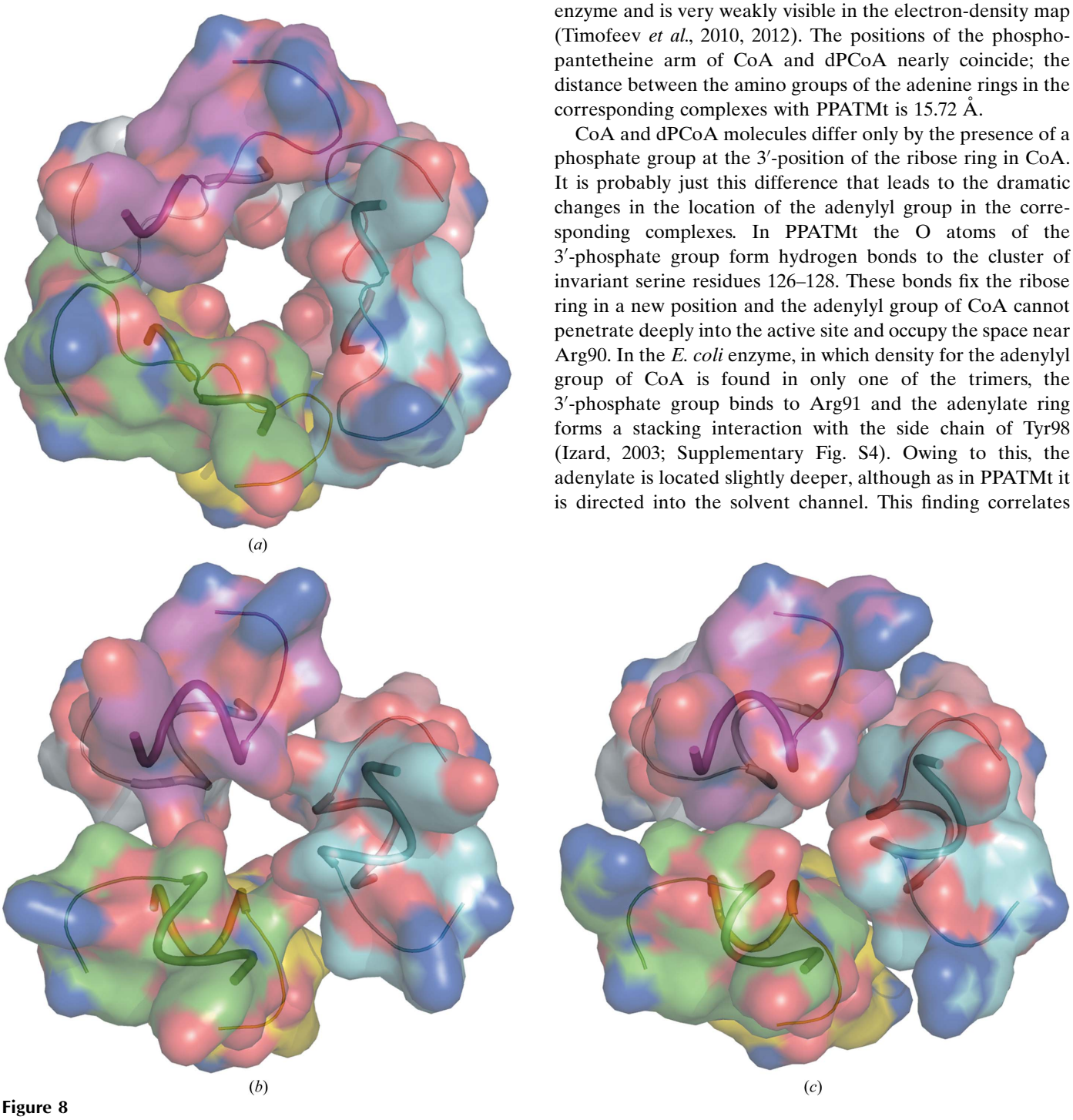

Figure 8
The surroundings of the solvent-filled channel in the different forms of PPAMt: (*a*) apoenzyme, (*b*) PPATMt–ATP and (*c*) PPATMt–dPCoA. The regions 89–96 of the PPATMt hexamer situated along the channel perimeter are shown as a surface representation. The surface is coloured according to atom type.

well with the higher affinity of CoA for PPATEc: the latter is copurified with 0.5 *M* tightly bound CoA per PPAT monomer (Geerlof *et al.*, 1999; Miller *et al.*, 2007). This allows us to suggest that the conformational changes in the molecule of PPATMt are induced by the movement of Arg90. When the adenylyl group binds close to Arg90 its side chain leaves its previous position to form favourable hydrogen bonds to the α-phosphate of dPCoA or to the β- and γ-phosphates of ATP.

The comparison of X-ray structures of PPATMt complexes with functional ligands shows that the transformation of irregular loop into helix in a single subunit which occurs upon ligand binding influences the structure of a whole hexameric molecule of the enzyme. In Fig. 8 the surroundings of the solvent-filled channel in the apo form (Fig. 8*a*), the PPATMt–ATP complex (Fig. 8*b*) and the PPAT–dPCoA (Fig. 8*c*) complex are shown as surface representations. These pictures represent the changes in the state of the PPAT molecule at several steps of the reaction: free enzyme, enzyme with bound substrate and enzyme with bound reaction product. We can observe that because of changes in quaternary structure the diameter of the solvent-filled channel is different in the different forms of the enzyme. Similar variations of the inner diameter of the channel in PPATMt have been found upon binding of the ATP analogue AMPcPP (Wubben & Mesecar, 2010).

There are several amino-acid residues situated along the channel perimeter or close to it whose movement is directly responsible for the changes in the channel diameter (Fig. 5). All of these residues, Arg90, Thr91, Thr93, Asp94 and Glu96, belong to the region 89–96. In the apoenzyme the side chains of Glu96 and Asp94 are exposed into the channel. The repulsion between the negative-charged residues can promote expansion of the channel. Upon the binding of ATP and the movement of Arg90 hydrogen bonds are formed between the carboxylic O atoms of Glu96 and Asp94 and the main-chain N atoms of Gly92, Thr91 and Thr93 of the neighbouring subunit. Thus, the local negative charge inside the channel near the trimer interface is reduced. In PPAT–dPCoA Glu96 is bound to Gly92 and Thr91 in the same subunit, all intersubunit hydrogen bonds along the channel perimeter are broken and the side chain of Thr93 is exposed to the channel. It turns out that the hexameric PPAT molecule oscillates during the reaction cycle; the diameter of the inner channel narrows and expands periodically during reaction owing to rearrangement of the hydrogen-bond system. Therefore, the action of PPATMt is accompanied by a variation in the local charge near the trimer interface which leads to the changing inner channel diameter. The largest diameter of the channel is found in the apoenzyme, in which six Glu96 and Asp94 residues are directed into the channel.

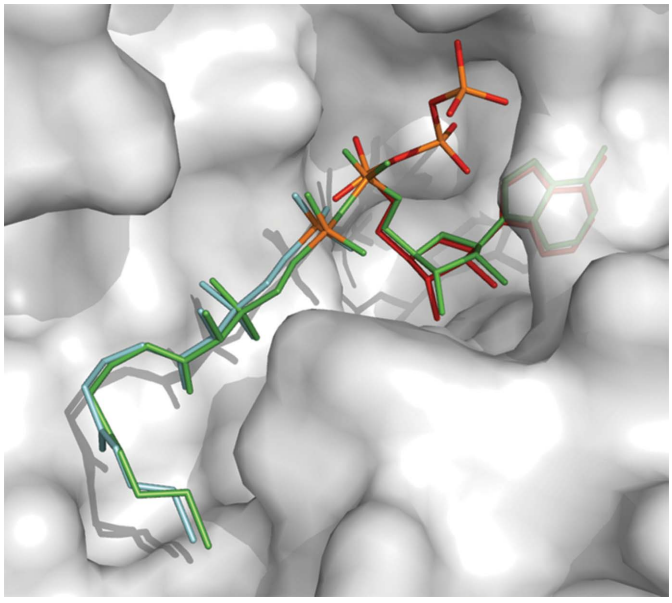

Figure 9
The arrangement of PhP (blue sticks), ATP (red sticks) and dPCoA (green sticks) in the active site of PPATMt. P atoms are coloured orange. The molecule of PPATMt is shown in surface representation. Superposition on C^{α} atoms of the structures of PPAT–PhP (PDB entry 3nbk), PPAT–dPCoA (PDB entry 3rba) and PPAT–ATP (PDB entry 3uc5).

According to the results of biochemical and structural studies, the reaction between phosphopantetheine and ATP catalyzed by enzymes of the PPAT family proceeds by an in-line attack by the electrophilic phosphate of 4′-phosphopantetheine on the α-P atom of ATP without forming any intermediate between the substrates and the functional groups of the enzyme (Izard & Geerlof, 1999; Izard, 2002; Wubben & Mesecar, 2010). The role of the enzyme is in providing accommodation of the ligands in the most favourable position for reaction in order to reduce the activation energy of the transition state. This assumption is confirmed clearly by comparison of the three-dimensional structures of PPAT complexed with both substrates (ATP and PhP) and the reaction product dPCoA (Fig. 9). The position of the attacking P atom of 4′-phosphate in the substrate (PhP) practically coincides with its position in the product (dPCoA), while the distance between the α-P atom of the adenylyl group of ATP attacked by PhP and its position after reaction in dPCoA is less than 0.5 Å. The slight difference in the positions of the reactive groups before and after reaction is in good agreement with the in-line displacement reaction mechanism.

The protein-crystallization experiments on the International Space Station 'JAXA PCG-Crystallizer' were supported by the Central Scientific Research Institute of Machine-Building of the Russian Federal Space Agency (Roscosmos). We thank our Japanese colleagues M. Sato, K. Ohta, H. Tanaka, K. Inaka and their coworkers for helpful advice, loading and assembling the JCB crystallization box and assistance in collecting X-ray diffraction data sets at the SPring-8 synchrotron-radiation facility.

References

Abkido, Y. (1967). *Biochemistry*, **61**, 290–299.
Adams, P. D., Grosse-Kunstleve, R. W., Hung, L.-W., Ioerger, T. R., McCoy, A. J., Moriarty, N. W., Read, R. J., Sacchettini, J. C., Sauter, N. K. & Terwilliger, T. C. (2002). *Acta Cryst.* D**58**, 1948–1954.
Badger, J. *et al.* (2005). *Proteins*, **60**, 787–796.

Begley, T. P., Kinsland, C. & Strauss, E. (2001). *Vitam. Horm.* **61**, 157–171.
Bork, P., Holm, L., Koonin, E. V. & Sander, C. (1995). *Proteins*, **22**, 259–266.
Bradford, M. M. (1976). *Anal. Biochem.* **72**, 248–254.
Brown, K. L., Morris, V. K. & Izard, T. (2004). *Acta Cryst.* D**60**, 195–196.
Edwards, T. E., Leibly, D. J., Bhandari, J., Statnekov, J. B., Phan, I., Dieterich, S. H., Abendroth, J., Staker, B. L., Van Voorhis, W. C., Myler, P. J. & Stewart, L. J. (2011). *Acta Cryst.* F**67**, 1032–1037.
Emsley, P. & Cowtan, K. (2004). *Acta Cryst.* D**60**, 2126–2132.
García-Ruiz, J. M. (2003). *Methods Enzymol.* **368**, 130–154.
García-Ruiz, J. M. & Moreno, A. (1994). *Acta Cryst.* D**50**, 484–490.
Geerlof, A., Lewendon, A. & Shaw, W. V. (1999). *J. Biol. Chem.* **274**, 27105–27111.
Izard, T. (2002). *J. Mol. Biol.* **315**, 487–495.
Izard, T. (2003). *J. Bacteriol.* **185**, 4074–4080.
Izard, T. & Geerlof, A. (1999). *EMBO J.* **18**, 2021–2030.
Jackowski, S. & Rock, C. O. (1984). *J. Bacteriol.* **158**, 115–120.
Kuranova, I. P., Smirnova, E. A., Abramchik, Y. A., Chupova, L. A., Esipov, R. S., Akparov, V. K., Timofeev, V. I. & Kovalchuk, M. V. (2011). *Crystallogr. Rep.* **56**, 884–891.
Lamprecht, W. & Trautschold, J. (1974). *Methods of Enzymatic Analysis*, 2nd ed., edited by H. U. Bergmeyer, Vol. 4, pp. 2127–2131. New York: Academic Press.
McCoy, A. J., Grosse-Kunstleve, R. W., Storoni, L. C. & Read, R. J. (2005). *Acta Cryst.* D**61**, 458–464.
Miller, J. R., Ohren, J., Sarver, R. W., Mueller, W. T., de Dreu, P., Case, H. & Thanabal, V. (2007). *J. Bacteriol.* **189**, 8196–8205.
Morris, V. K. & Izard, T. (2004). *Protein Sci.* **13**, 2547–2552.
Murshudov, G. N., Skubák, P., Lebedev, A. A., Pannu, N. S., Steiner, R. A., Nicholls, R. A., Winn, M. D., Long, F. & Vagin, A. A. (2011). *Acta Cryst.* D**67**, 355–367.
Otwinowski, Z. & Minor, W. (1997). *Methods Enzymol.* **276**, 307–326.
Robishaw, J. D. & Neely, J. R. (1985). *Am. J. Physiol.* **248**, E1–E9.
Rock, C. O., Park, H.-W. & Jackowski, S. (2003). *J. Bacteriol.* **185**, 3410–3415.
Rossmann, M. G., Liljas, A., Brändén, C. I. & Banaszak, I. J. (1975). *The Enzymes*, 3rd ed., edited by P. D. Boyer, Vol. 11, pp. 62–102. New York: Academic Press.
Sato, M. *et al.* (2006). *Microgravity Sci. Technol.* **18**, 184–189.
Suzuki, T., Abiko, J. & Shimizu, M. (1967). *J. Biochem.* **62**, 542–549.
Takahashi, H., Inagaki, E., Fujimoto, Y., Kuroishi, C., Nodake, Y., Nakamura, Y., Arisaka, F., Yutani, K., Kuramitsu, S., Yokoyama, S., Yamamoto, M., Miyano, M. & Tahirov, T. H. (2004). *Acta Cryst.* D**60**, 97–104.
Takahashi, S., Tsurumura, T., Aritake, K., Furubayashi, N., Sato, M., Yamanaka, M., Hirota, E., Sano, S., Kobayashi, T., Tanaka, T., Inaka, K., Tanaka, H. & Urade, Y. (2010). *Acta Cryst.* F**66**, 846–850.
Tanaka, H., Inaka, K., Sugiyama, S., Takahashi, S., Sano, S., Sato, M. & Yoshitomi, S. (2004). *J. Synchrotron Rad.* **11**, 45–48.
Timofeev, V. I., Smirnova, E. A., Chupova, L. A., Esipov, R. S. & Kuranova, I. P. (2010). *Crystallogr. Rep.* **55**, 1050–1059.
Timofeev, V. I., Smirnova, E. A., Chupova, L. A., Esipov, R. S. & Kuranova, I. P. (2012). *Crystallogr. Rep.* **57**, 96–104.
Worrall, D. M. & Tubbs, P. K. (1983). *Biochem. J.* **215**, 153–157.
Wubben, T. J. & Mesecar, A. D. (2010). *J. Mol. Biol.* **404**, 202–219.
Wubben, T. & Mesecar, A. D. (2011). *Acta Cryst.* F**67**, 541–545.
Yoon, H.-J., Kang, J. Y., Mikami, B., Lee, H. H. & Suh, S. W. (2011). *Mol. Cells*, **32**, 431–435.
Zhao, L., Allanson, N. M., Thomson, S. P., Maclean, J. K. F., Barker, J. J., Primrose, W. U., Tyler, P. D. & Lewendon, A. (2003). *Eur. J. Med. Chem.* **38**, 345–349.